Assessment of vapour chamber heat spreader implementation for avionic module thermal management

International Journal of Thermal Technologies
E-ISSN 2277 – 4114

Available at http://inpressco.com/category/ijtt/

Research Article

Assessment of Vapour Chamber Heat Spreader Implementation for Avionic Module Thermal Management

Andy Jones†*, Rui Chen† and Angus Murray‡

†Department Automotive and Aeronautical Engineering, Loughborough University, Leicestershire, LE11 3TU, UK
‡BAE Systems Military Air & Information, Warton, Lancashire, PR4 1AX, UK

Accepted 09 May 2016, Available online 01 June 2016, **Vol.6, No.2 (June 2016)**

Abstract

Thermal management of aircraft heat loads is quickly becoming a limiting factor of vehicle performance and reliability. This paper details improvements in forced-convection cooled avionic module heat removal efficiency with the implementation of two-phase high thermal conductivity Vapour Chamber Heat Spreaders (VCHS). A bespoke test rig provides experimental thermal comparisons of an aluminium and embedded VCHS avionic heat exchanger. The experimental results validate a numerical thermal resistance network, which is utilised to simulate more representative avionic chassis geometries. The VCHS dramatically reduces thermal variation in circuit card and avionic heat exchanger exhaust temperatures. Increased isothermalisation of the heat exchanger greatly increases effective heat transfer area in comparison to a traditional aluminium chassis. The VCHS acts as a very effective thermal buffer between the avionic circuit cards and coolant airflow, allowing a more predictable avionic thermal behaviour irrespective of circuit card architecture. The improved heat rejection capability allows either a substantial increase in avionic growth capacity (increased power output for a fixed exhaust temperature) or a substantial reduction in mass flow rate (reduced demand on vehicle thermal management system). An avionic growth capacity of up to 58% is achieved with representative thermal loading conditions.

Keywords: *Avionic Thermal Management, Two-Phase Heat Transfer, Experimental Analysis, Thermal Modelling, Vapour Chamber Heat Spreader*

1. Introduction

Modern military aircraft heat loads are increasing at an exponential rate (Walters *et al*. 2010; Iden 2012). Thermal management of these heat loads is becoming increasingly difficult due to the requirement to reduce aircraft thermal signature and maximise efficiency of fuel burn. Avionic heat loads are a particularly difficult area of thermal management which is rapidly expanding through increased airframe operational capability through improved weapons systems, communications, guidance and interoperability with other aircraft.

Avionic thermal management presents an additional layer of complexity due to the interface management between the airframe manufacturer and avionic equipment suppliers. The airframe manufacturer places a high dependence on equipment suppliers for isolated avionic development (Chiang 1999). The equipment supplier specifies an interface requirement of avionic airflow rate and temperature at module inlet; the circuit card architecture and operating conditions within the module are often Intellectual Property Rights (IPR) of the supplier. The airframe manufacturer is required to provide the specified cooling capacity with a limited ability to accurately determine circuit card temperatures. As no single party has access to the complete data set, a knowledge gap is generated. Avionic reliability is prioritised by the airframe manufacturer and cooling mass flow rates are often over specified through the application of additional safety factors to mask any unknown thermal behaviour. The oversupply of avionic cooling mass flow rate increases demands on the aircraft Thermal Management System and ultimately fuel consumed by the aircraft (Del valle & Blazquez Munoz 2014).

High rates of avionic failure are a feature of fast jet combat aircraft as a consequence of the increasing complexity of aircraft mission systems (Pearson & McCoy 2011). Without the ability to determine localised avionic temperatures, the airframe manufacturer can only assume that any avionic thermal failure is a saturation of total heat rejection capability. This is often resolved by additional coolant mass flow rate at further cost to the TMS. However, avionic thermal failures can also be attributed to the generation of isolated thermal hotspots within the

*Corresponding author: **Andy Jones**

module. Thermal failures are notoriously difficult to diagnose, often displaying minimal irreversible damage and clouded by the frequency of No Fault Found (NFF) failures in avionic equipment. A NFF failure is categorised as an operational failure that cannot be replicated or isolated in further testing or component analysis. This phenomenon is a serious consideration within the aerospace industry, contributing to more than 85% of all observed operational failures in aircraft electronics, costing over $10,000,000 each year in exchanging avionic units due to this failure mechanism (Söderholm 2007; Williams *et al*. 1998; Steadman *et al*. 2002).

The objective of this paper is to demonstrate a technology which allows the airframe manufacturer to more accurately determine localised thermal conditions of the avionic module, without the requirement for more detailed architectural information of internal circuitry. The ability to efficiently manage avionic heat loads can be utilised to improve airframe capability in one of two ways.

- Reduction in TMS fuel consumption: Avionic averaged heat rejection requirement can be more accurately specified, reducing mass flow rate demand from the TMS subsequently improving the vehicle fuel efficiency.
- Avionic growth capability: Optimisation of avionic heat loads to operate the module closer to the thermal design limit through the increase in power output; an increase in avionic growth capacity.

1.1 Avionic Thermal Management

Forced convection cooled avionic module heat rejection is completed through the process of conduction to cold wall cooling. Structural heat exchangers are embedded within the aluminium avionic chassis and forced convection cooling is utilised to generate a cold wall which the circuit cards are thermally coupled with. The conduction to cold wall design is of inherently high thermal resistance as the energy flow path consists of several material interfaces, multiple conduction processes and a forced convection process. A schematic of conduction to cold wall cooled circuit card is seen Figure 1 (Strattan 1983).

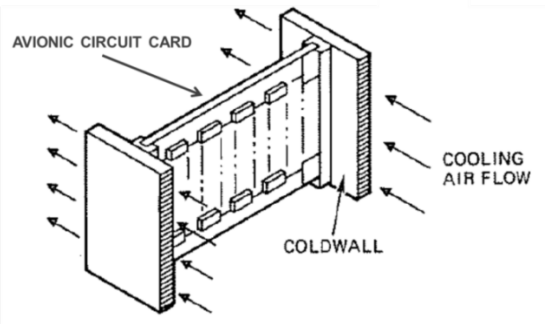

Fig.1 Conduction to cold wall avionic cooling process

Forced convection cooling is typically unsuitable for high power density applications due to the low specific heat capacity and poor thermal conductivity of air. However, the conduction to cold wall remains highly popular within the aviation industry due to the reliability, weight, cost, failsafe performance and simplicity of the technique. Air is deemed a reliable coolant as the penalty of a system leak within the airframe is minimised and during a TMS failure additional airflow can be supplied from the ambient environment.

Conduction to cold wall modules offer no direct contact between the coolant and active avionic component, thus negating the possibility of contamination from debris suspended within the airflow; typically a problem with runway pickup. The modules feature low a Fins Per Inch (FPI) straight channel heat exchanger design, reducing the module pressure drop and evading the risk of heat exchanger clogging. The active components are physically coupled to the heat exchanger wall and therefore still offer some heat rejection at natural convection and reduced flow rate conditions. Other cooling techniques such air impingement cooling, flow through cooling, and jet impingement cooling can offer an increase in thermodynamic efficiency, however these architectures feature no direct thermal coupling between the active components and avionic chassis heat exchanger (Mudawar 2001; Franklin & Charles 1983). These cooling techniques are very sensitive to a reduction in cooling mass flow rate and demonstrate extremely poor performance in natural convection conditions. It is an essential criterion that the avionics must operate with a reduced airflow supply; as in the event of an ECS failure the pilot, cabin environment and flight critical components are prioritised.

Thermal analysis of six circuit cards mounted within a ½ ATR (Air Transport Rack) module is displayed with the minimum, maximum and average component temperature of each circuit card presented as a percentage of avionic heat exchanger exhaust air temperature is presented in Figure 2 (Maxwell *et al*. 2010). It can be seen that while circuit cards 3, 4 & 5 display a close relationship between minimum and maximum component temperature, circuit card 6 demonstrates localised conditions operating 38.6% hotter than avionic exhaust airflow. The generation of a thermal hotspot is the result of high heat path thermal resistance and subsequently leads to irregular heat exchanger thermal loading. The relatively low thermal conductivity of an aluminium heat exchanger is unable to efficiently spread thermal energy reducing fin utilisation and diminishing heat removal efficiency with increasing mass flow rate. The theory presented in this investigation is that the reliability of an avionic module is actually based on the ability to handle isolated thermal hotspots as opposed to the saturation of total heat rejection capacity.

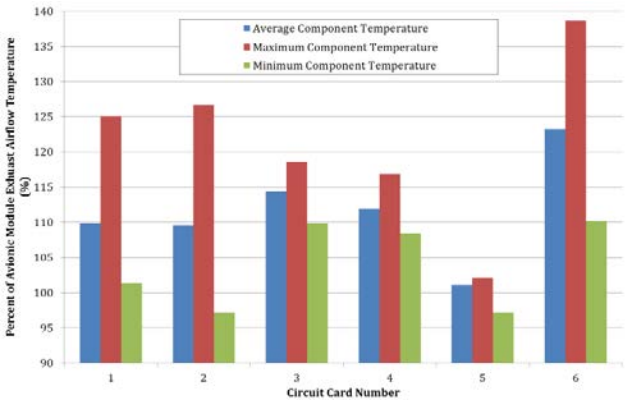

Fig.2 Thermal analysis of 'in-service' avionic module circuit card temperatures

Based on the operational data of Figure 2, to provide an adequate cooling capacity for circuit card 6 with fixed heat exchanger geometry would be to over cool circuit cards 1-5. This is a prime example of the lack of flexibility of avionic chassis and heat exchanger design. Avionic module over cooling increases the demand on aircraft cooling capacity exponentially increasing TMS fuel energy requirement (Allison *et al*. 2016).

The aim of this paper is to improve avionic heat exchanger thermal efficiency and avionic thermal reliability through the increased isothermalisation of the avionic heat exchanger. It will be shown that the proposed solution does improve heat exchanger efficiency, while maintaining the fundamental benefits of the conduction to cold wall forced convection avionics, protecting the IPR of equipment suppliers and allowing a better integration of avionic cooling with the aircraft TMS.

2. Methodology

For operational reasons, the heat exchanger geometry, module size, airflow rate, airflow temperatures, inlet and exhaust geometry, circuit card architecture, power output and chassis fixings mechanisms remain fixed. The proposed technology is the implementation of structurally embedded Vapour Chamber Heat Spreaders (VCHS) within the avionic chassis to act as a baseplate for the integral chassis heat exchanger. A VCHS is effectively a flat plate heat pipe, designed to utilise the efficient heat transportation of a two phase cycle to generate a flat plate of high thermal conductivity. The VCHS is implemented to provide a more uniform temperature distribution across the width of the heat exchanger baseplate. A VCHS schematic diagram can be seen in Figure 3 (Tsai *et al*. 2013).

As with heat pipes, a heat source is used to evaporate the working fluid to a vapour, which is transported to a heat sink by an internal pressure gradient. The heat sink condenses the vapour back to a fluid, which is returned to the heat source through capillary pumping forces to repeat the cycle.

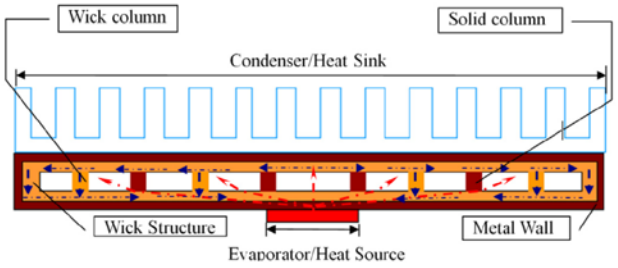

Fig.3 Vapour Chamber Heat Spreader schematic diagram

The primary function of a VCHS is the efficient transportation of heat energy from a single isolated source to a large heat sink. This passive two phase cooling cycle creates a plate ideal for avionic applications. The capillary pumping forces through the wick ensure the cooling cycle operation in negative G applications. The sealed unit has no risk of performance degradation through a supply or sealing issue. Most importantly the implementation of an embedded VCHS within an avionic chassis offers minimal disruption to conduction to cold wall cooling technique (Reyes *et al*. 2012; Jaworski 2012; Naphon & Wiriyasart 2012).

The performance of VCHS for avionic heat rejection is assessed both experimentally (with a bespoke test rig) and numerically (with the use of a thermal resistance network). The experimental rig heat exchanger is based on a genuine avionic module. To facilitate a back-to-back material comparison, interchangeable VCHS and Aluminium plates are inserted in the same test rig. This design requirement forced a number of additional material interfaces which are not present with a genuine avionic module and act to further increase the total heat flow path thermal resistance. To combat this, the experimental data will be used to validate a thermal resistance network, which can predict the performance of an aluminium and VCHS avionic chassis with the correct geometry and thermal resistance. Both approaches are used to determine the applicability of VCHS for conduction to cold wall cooling and assess the potential performance improvement in avionic heat exchanger efficiency.

2.1 Experimental Test Setup

A sample VCHS (H,W,D: 122mm,87mm,3mm) has been supplied for this investigation and an equally sized aluminium plate has been machined, allowing the materials to be directly interchangeable. The VCHS plates are a pressed copper housing with a sintered copper dust wick structure. The fill ratio is one third and the working fluid is distilled water.

A bespoke test plate has been designed for the purpose of quantifying the heat transfer efficiency of the two materials; a schematic can be seen in Figure 4. The geometry and fin design of the test plate has been matched exactly to a genuine in service avionic module

heat exchanger, with the exception of an increased thickness of 3mm to the top plate to allow the implementation of the two test plates.

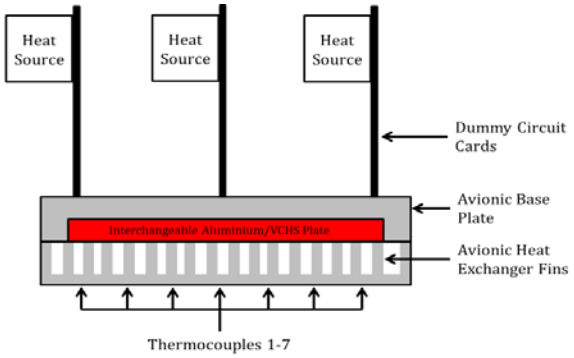

Fig.4 Experimental rig schematic diagram

Experimentally, the power output and cooling flow characteristic will be supplied as per in-flight operation of these avionic modules. Typically, a chassis of this size would exhibit a power output of 60Watts to 140Watts depending on application, with a corresponding mass flow rate of 15kg/hr to 35kg/hr at an inlet temperature of 15ºC to 20ºC.

A mass flow rate is supplied at ambient laboratory temperature from an air fan with integrated smooth bell mouth inlet and venturi. The bell mouth inlet and venturi are used to ensure a measured and calibrated mass flow is supplied to the avionic chassis. The mass flow rate is calculated by measuring the pressure differential between the fan inlet throat and ambient air, assuming no losses across the smooth bell mouth intake.

In order to replicate the conduction to cold wall cooling process, heating elements are thermally coupled to the circuit card which is mounted against the chassis cold wall. The rig allows a number of circuit cards to be used, with a comparison being made across three cards in this investigation. The heater power output is controlled by a variable desktop power supply. All data acquisition channels are calibrated previous to testing. Temperature readings are taken with both individual thermocouples and a manufacturer calibrated thermal camera (FLIR Systems 2016). Thermocouples will be used to measure the inlet airflow, component and exhaust airflow temperatures in seven locations equally spaced across the width of the heat exchanger.

2.2 Thermal Resistance Network

A thermal resistance network is used to predict the avionic module chassis thermal performance of a geometrically correct aluminium and VCHS chassis. The first requirement is to establish the thermal conductivity of both materials; this data is collected experimentally with a thermal camera. Both materials are subjected to a heat source of variable power, with an area of 0.00075m^2 and the plates are suspended within the ambient lab environment. The stabilised temperature of each plate is filmed to interrogate the thermal degradation across the plate. A back-to-back comparison of a 30Watt thermal load is shown in Figure 5. The measured thermal conductivity from this test shows the VCHS plate at 1481W/mK and the Aluminium plate at 206W/mK.

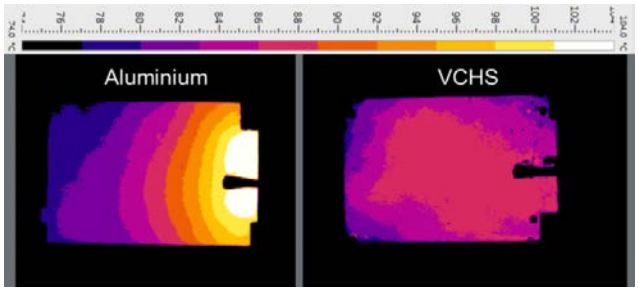

Fig.5 Thermal image of a VCHS and Aluminium plates

The aluminium plate demonstrates a lower thermal conductivity, presenting a clearly defined localised hotspot around the heat source. The material temperature reduces linearly from this point, across the length of the plate. The VCHS presents a more equal temperature distribution, demonstrating a lower maximum temperature and a higher minimum temperature than the aluminium plate. The measured thermal conductivity of both plates across a range thermal loading is detailed in Figure 6. It is seen that as the power output increases, the thermal conductivity of the aluminium plate remains constant while the thermal conductivity of the VCHS plate increases exponentially to a maximum of 7876W/mK.

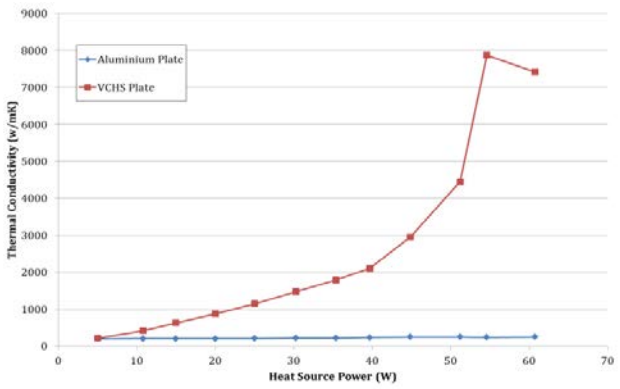

Fig.6 Measured thermal conductivity of Aluminium and VCHS plates

The thermal conductivity of a VCHS is dependent on the power applied to it; the greater the power, the higher the evaporator temperature, increasing the rate of working fluid phase change and the internal pressure gradient. The resulting increase of vapour flow rate within the VCHS increases the rate of thermal transportation and therefore thermal conductivity. As

the power continues to increase, the thermal conductivity increases until the VCHS reaches a physical limitation such as the sonic, boiling, entrainment or capillary limit. The test in Figure 6 details a plate which is believed to have reached its capillary limit at 63Watts; corresponding to an evaporator temperature of 115ºC. At this point the input heat flux limit is surpassed and vaporisation at the evaporator exceeds the rate at which fluid can return from the condenser. Working fluid is not available at the evaporator to absorb thermal energy and it dries out. It is seen from this data that this VCHS plate will safely operate with a thermal conductivity of 5000W/mK; over 24 times that of aluminium. The measured thermal conductivity of the VCHS in response to given heat flux is utilised in the model based on the temperature differential between the evaporator and condenser.

The thermal resistance network schematic for a single circuit card can be seen in Figure 7, the following section details the governing equations. The temperature differential, ΔT, across a heat transfer process is defined as the product of the rate of heat transfer,$\dot{Q}$, and thermal resistance, R, of that process.

$$\Delta T = \dot{Q}R \tag{1}$$

A thermal resistance is dependent on the type of heat transfer; conduction, convection or radiation. The thermal resistance of a radiative heat transfer process, R_{Rad}, is based on the radiative heat transfer coefficient, h_{rad}, and the surface area of heat transfer, A_s.

$$R_{rad} = \frac{1}{h_{rad}\ A_s} \tag{2}$$

Where the radiative heat transfer coefficient is the product of the emissivity coefficient, ε, Stefan-Boltzmann constant, σ, heat transfer area, $A_s$and a function of the temperature differential between the heat transfer surface, T_s, and the surroundings, T_{surr}.

$$h_{rad} = \varepsilon\,\sigma\,A\left({T_s}^2 - {T_{surr}}^2\right)(T_s + T_{surr}) \tag{3}$$

A conductive resistance, R_{cond}, is defined as the length of heat conduction divided by the product of the material thermal conductivity, K, and the area of which the heat is travelling through, A.

$$R_{Cond} = \frac{L}{K\,A} \tag{4}$$

The avionic chassis heat flow path features a number of material interfaces which interrupt the heat transfer; circuit card to avionic chassis for example. The contact interface of two materials can be modelled as the summation of contact and gap conductance. The total joint conductance is a function of surface roughness, material hardness, clamping pressure and thermal conductivities of materials and material voids (air). A thermal paste is used as a Thermal Interface Material (TIM) to increase total joint thermal conductance and to improve the estimation of contact thermal resistance. Assuming the paste behaves like a liquid and fills all air gaps between the two materials, the thermal conductivity of the paste can be substituted in the gap conductance relationship. The distance between the two material is assumed as the surface roughness for a milled section of aluminium (Teertstra *et al*. 1997).

A convective thermal resistance, R_{Conv}, is based on the convective heat transfer coefficient, h_{conv}, and the convection surface area.

$$R_{Conv} = \frac{1}{h_{conv}\,A_s} \tag{5}$$

Where the convective heat transfer coefficient is defined as the product of the Nusselt number, N_u, and material thermal conductivity divided by the length of heat exchange area (fin, channel), L.

$$h_{conv} = \frac{N_u\,K}{L} \tag{6}$$

The Nusselt number is a non-dimensional ratio of convective heat transfer to conductive heat transfer across a boundary. The Nusselt number can be approximated by the Dittus-Boelter equation for turbulent airflows. The approximation for heating of a fluid is defined as a function of Reynolds number, R_e, and Prandtl number, P_r.

$$N_u = 0.0023{R_e}^{4/5}{P_r}^{0.4} \tag{7}$$

Where Reynolds number is a non-dimensional characterisation of fluid flow behaviour and can be defined as the product of the fluid density, ρ, velocity, u, and channel length divided by the fluid viscosity, μ. The Prandtl number is a non-dimensional ratio of fluids momentum diffusivity to its thermal diffusivity and can be defined as the is the product of the fluid viscosity and specific heat capacity, C_p, divided by the thermal conductivity, K.

$$R_e = \frac{\rho\,u\,L}{\mu} \tag{8}$$

$$P_r = \frac{\mu\,C_p}{K} \tag{9}$$

As mass flow rate throughout the test is variable, from 15kg/hr to 35kg/hr, and assuming an even distribution across the 17 heat exchanger fins, channel airflow velocity ranges from 8m/s to 23m/s. Channel flow condition ranges from upper transitional to fully developed turbulent flow and therefore some inaccuracy is expected from the Dittus-Boelter approximation of Nusselt number; leading to an incorrect convective heat transfer coefficient. The initial network is set to replicate the experimental conditions and a measured convective heat transfer coefficient will be determined as the plate heat

rejection, Q, divided by the product of the channel area, A, and temperature differential between the surface temperature, T_s, and airflow free stream temperature, T_∞. The measured convective heat transfer coefficient will be used to generate a correction factor which is applied to the calculated convective heat transfer coefficient.

$$h_{exp} = \frac{Q}{A\,(T_s - T_\infty)} \tag{10}$$

The module exhaust temperature is averaged from the seven localised temperature readings and the plate heat rejection is calculated as the product of the channel mass flow rate, $\dot{m}$, the specific heat capacity of the fluid, C_p, and the temperature differential of airflow at inlet, T_{in}, and exhaust, T_{ex}.

$$Q = \dot{m}\ C_p(T_{ex} - T_{in}) \tag{11}$$

The avionic module heat flow path is essentially an amalgamation of the thermal resistances detailed above. Depending on the configuration, some heat transfer is considered to be simultaneous (in which case thermal resistances are in parallel) and some heat transfer is considered to be consecutive (in which case thermal resistances are in series). When calculating a thermal resistance in series, as with electrical resistances, the total resistance, R_{total}, is the sum of the individual resistances, $R_{1,2,3,x}$. When calculating a thermal resistance is parallel, the total resistance is defined as. Please see the reference citing style i.e. how the references are to be written as described below.

$$\frac{1}{R_{Total}} = \frac{1}{R_1} + \frac{1}{R_2} \tag{12}$$

The thermal network calculates seven exhaust air temperatures which correspond to the location of the seven thermocouples of the experimental set up. This allows the interrogation of localised and averaged plate heat transfer condition to define the state of plate isothermalisation. Once the network is validated against experimental data, the calculations are adapted to predict the system energy flow for a geometrically correct module.

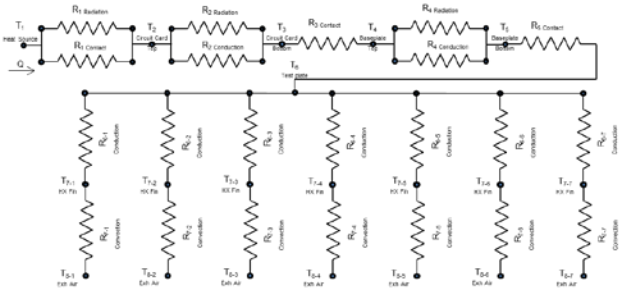

Fig.7 Single heat source thermal resistance network of schematic diagram shown in Figure 4

The network is then adapted for multiple heat sources to more accurately replicate the conditions of the genuine component. Additional heat sources are replicated by the duplication of T1 through T6 for each heat source location. The ability to simulate unequal thermal loading across the avionic base plate allows the replication of real life conditions displayed in Figure 2.

3. Results and Discussion

3.1 Experimental Comparison

Initially both avionic chassis are tested with a single circuit card mounted at the extremity of the base plate in the orientation of cooling airflow. The small heat transfer area generated by a single card replicates a significant thermal hotspot. Figure 8 demonstrates the reduction in airflow temperature with increasing distance from the heat source for both aluminium and VCHS. Local temperature data is presented as a percentage of maximum airflow temperature at various mass flow rates for a single heat source. The VCHS base plate clearly demonstrates a more uniform temperature distribution across the width of the avionic base plate. It is also seen that by increasing the mass flow rate, the range of temperature distribution becomes greater.

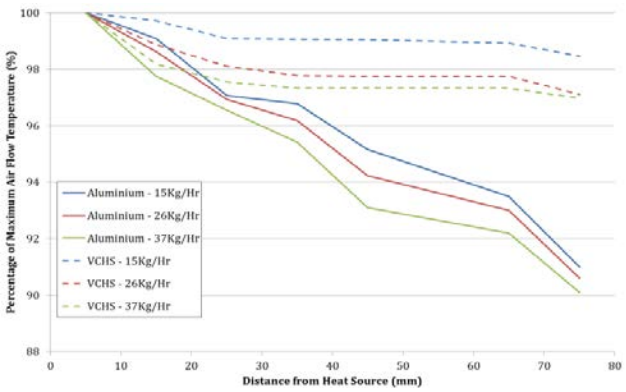

Fig.8 Localised temperatures presented as a percentage of the maximum recorded temperature

The improved thermal conductivity of the VCHS base plate is directly responsible for a reduction in component temperature across all comparative mass flow rates and thermal loads, as seen in Figure 9. It can be seen that the avionic exhaust temperature profile falls on a curve with increasing mass flow rate. As a result, a small temperature reduction equates to a large mass flow rate reduction. For example, when considering a fixed component temperature of 55ºC, Figure 9 demonstrates a mass flow of 37.2kg/hr is required for an aluminium plate. A comparative 14.2kg/hr is required for the VCHS, equating to a mass flow reduction of over 65%. The reduction in mass flow rate for a fixed component temperature is as a result of an increased heat exchanger effective area.

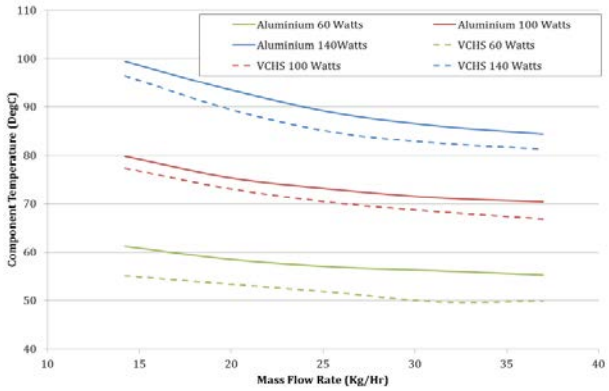

Fig.9 Component response to a mass flow rate sweep

The supply of an increasing mass flow rate is exponentially expensive for the TMS and provides diminishing returns from the low FPI heat exchanger channels. This demonstrates how attempting to thermally condition a single isolated hotspot with increased mass flow rate can be detrimental to TMS and aircraft fuel efficiency.

3.2 Thermal Network Validation

The thermal network and experimental data are compared in Figure 10. This data displays temperature readings from four separate airflow locations with two differing heat sources applied to both materials at a range of five mass flow rates to highlight the flexibility of the model. The correlation between the experimental and modelled temperatures is within 8% across all conditions tested. The model validation provides an accurate measure of Nusselt number correlation with experimental data across the upper transitional turbulent airflow conditions. As discussed, the limitation of the experimental testing is the ability to compare the two materials back-to-back in a geometrically correct environment. The experimental data is therefore only utilised for model validation and the remaining results are outputs of the thermal network model.

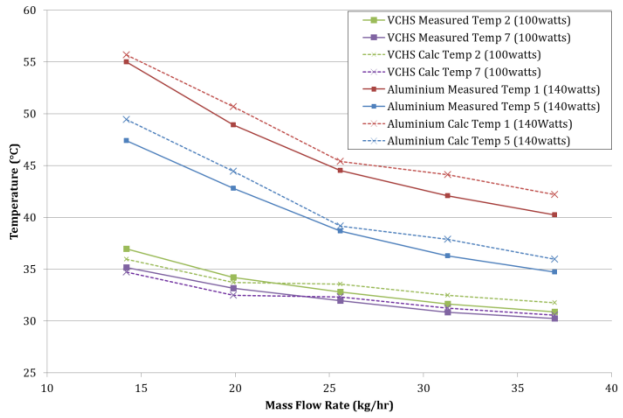

Fig.10 Experimental validation of thermal network

3.3 Equal Heat Source Loading

Initially, three equal temperature heat sources located at an equal distance from each other are considered, as shown in Figure 11. When considering an analysis of the avionic module with multiple heat sources of equal temperature, the flow path of thermal transportation is short. As the heat transportation lengths are short, the aluminium chassis is able to effectively utilise the majority of the heat exchanger area and the benefit of a high thermal conductivity VCHS is minimised. The majority of thermal resistance is generated through the avionic circuit card (aluminium) and material contact resistances 'upstream' of the avionic chassis. The fact that each heat source is equal means that no thermal hotspot is simulated in this case. The result is a uniform distribution of a lower peak temperature, subsequently reducing the temperature differential across VCHS and therefore plate thermal conductivity.

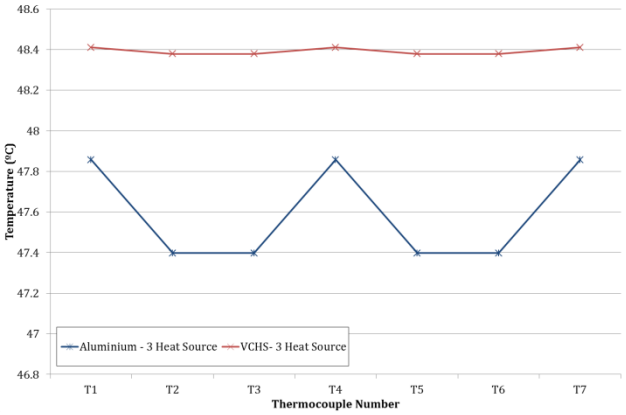

Fig.11 Equal thermal loading exhaust air temperature comparison

It is seen in Figure 11 that the exhaust airflow temperatures are higher for the VCHS plate, albeit within 2%. The higher the airflow temperature in this case shows a smaller temperature differential between heat source and coolant due to a lower the thermal resistance. When considering this thermal loading, the performance benefit of VCHS is small. As the total thermal resistance is very similar across both materials, avionic growth capacity is small. When considering a total of 140Watts spread evenly across three circuit cards an avionic growth capacity of 4% - 15% was found depending on mass flow rate.

3.4 Unequal Heat Source Loading

The operational avionic module data presented in Figure 2 suggests that in fact the heat source thermal loading is not equal. The temperature differential from the averaged circuit card temperature to the hottest circuit card temperature was found to be as high as 13ºC. These thermal loading conditions have been replicated for a more representative comparison of the two materials and the results can be seen in Figure 12. The power output of circuit card 2 and 3 are equal,

with the power output of circuit card 1 set to achieve a component temperature 13ºC higher than the average of 2 and 3. The high temperature circuit card is located at one side of the avionic chassis; as Figure 2. It can be seen that the peak circuit card temperatures are at the location of the highest thermal loading for both materials. The circuit card temperatures of the VCHS present a much smaller thermal variation across the width of the module. The peak temperature is substantially reduced as the thermal energy is efficiently spread across the heat exchanger base plate, increasing the effective heat transfer area and improving the averaged heat rejection capability of each airflow channel.

The VCHS essentially acts as a thermal buffer between the circuit cards and forced convection airflow. The function of a thermal buffer at the component thermal interface is highly desirable when considering the implementation within an airframe. The insensitivity of the VCHS to irregular thermal loading allows the equipment supplier to couple heat loads as required and the airframe integrator to operate on the basis of cooling an isothermal heat exchanger. IPR regarding the internal architecture of the module is not required and avionic heat load can be more accurately integrated into the TMS.

As the intensity of the thermal loading at circuit card 1 is increased, the VCHS will continue to passively increase the thermal conductivity of the plate. The ability to better match heat rejection capability (through improved heat exchanger fin utilisation) and heat rejection demand is a highly desirable behaviour; previously defined as a requirement for improving TMS efficiency and as a tool to withstand future avionic growth demands (Jones *et al*. 2016).

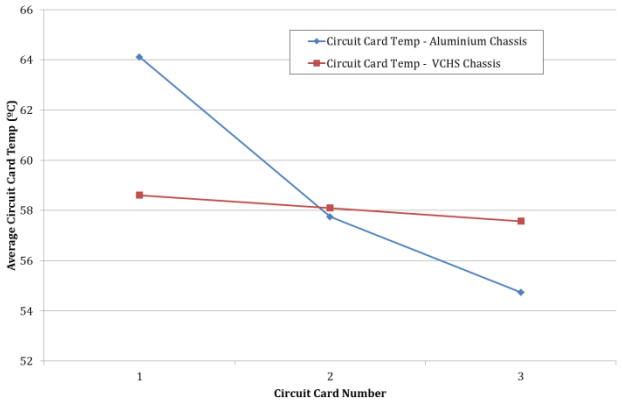

Fig12 Component temperatures with thermal loading conditions to replicate **Error! Reference source not found.**

When considering the avionic growth capacity, Figure 13 displays the avionic module exhaust temperatures for two thermal loading conditions.

The results are presented as a percentage of the localised temperature against the maximum recorded exhaust temperature. The thermal loading of the aluminium chassis remains constant with the results seen in Figure 12, while the VCHS chassis thermal loading is increased to the point at which the peak exhaust temperatures are equal at the location of airflow Temperature 1.

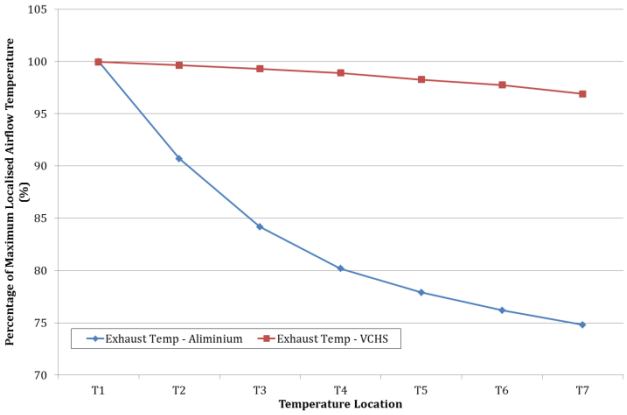

Fig.13 Module exhaust airflow as percentage of maximum localised temperature

The inlet mass flow rate and temperature remains constant along with the distribution of thermal loading; circuit card 2 and 3 are equal power outputs, with circuit card 1 replicating a hotspot. It is found that the VCHS module is able to accept 58% more thermal energy than the aluminium module in this test case. At this elevated thermal load, the airflow temperature variation is 3% across the heat exchanger, a large reduction compared to 25% variation of the aluminium. The ability to provide an isothermal heat exchanger increases the effectiveness of forced convection cooling and fin utilisation allowing the chassis to fully exploit the coolant. The ability to efficiently spread thermal energy and vary the thermal conductivity of the plate based on evaporator temperature allows the VCHS to be insensitive to thermal loading conditions and circuit card architecture. The key advantage to this behaviour is the ability to more accurately control and predict peak circuit card temperatures from measured airflow conditions to better specify coolant mass flow rate. The reduction of thermal hotspots is a further factor allowing a better integration of avionic heat loads into the TMS, fundamentally improving system efficiency and component reliability.

Conclusions

Considerable performance benefits are delivered from the implementation of VCHS in avionic module cooling. The improvement in heat exchanger isothermalisation increases effective heat transfer area and therefore heat rejection capability. The insensitivity of VCHS to heat source geometry, power output and mass flow rate allows it to act as an efficient technology for thermal interface management between heat source and coolant. The VCHS module allows the airframe manufacturer to better integrate the avionic subsystem, without the requirement for detailed IPR of

avionic circuit card architecture. It is considered that the improvement in subsystem integration to the wider thermal management system and the combined reliability improvement would be the primary strength of this technology.

The improved isothermalisation of the VCHS chassis reduces the thermal range of circuit card temperatures. The ability of all circuit cards to operate closer to an average temperature reduces the generation of isolated thermal hotspots and improves the plate averaged heat rejection. Reliability improvements are not specifically quantified in this study but are assumed; as the thermal failure of an avionic module through the total saturation of heat removal capacity occurs at a much greater thermal loading than the generation of a single hotspot. The improvement in thermal efficiency from the increased heat exchanger fin utilisation has been proved to be applicable to either a reduction in mass flow rate or an increase in avionic growth capability.

The final performance advantage of VCHS is the ability to passively control its thermal conductivity (and subsequently heat exchanger performance) with increasing thermal loading. This improves the ability to handle irregular and unknown circuit card power outputs; such as those found in genuine avionic modules.

Acknowledgements

The project is co-funded by EPSRC (Engineering and Physical Sciences Research Council, UK) and BAE Systems. The samples of 2 VCHS have been supplied from Meng-Chang Tsai at the Nuclear Energy Research Facility, Taiwan.

References

Allison, D.L., Alyanak, E.J. & Shimmin, K., 2016. Aircraft System Affects Including Propulsion and Air Cycle Machine Coupled Interactions. In 57th AIAA/ASCE/AHS/ASC Structures, Structural Dynamics, and Materials Conference. AIAA SciTech. San Diego, CA: American Institute of Aeronautics and Astronautics, pp. 1–16. Available at: http://dx.doi.org/10.2514/6.2016-0671.

Chiang, J.-T., 1999. Defense conversion and systems architecture: challenges to Taiwan's aircraft industry. Technology in Society, 21(3), pp.263–274. Available at: http://www.sciencedirect.com/science/article/pii/S0160791X99000147 [Accessed November 5, 2015].

FLIR Systems, 2016. FLIR A320 (30Hz) Thermal Camera Specification Sheet. Available at: http://support.flir.com/DsDownload/Assets/48201-0201_en_51.pdf [Accessed January 17, 2016].

Franklin, J.L. & Charles, F., 1983. Thermal Characteristics of Standardized Air Force Avionic Enclosures. In 13th Intersociety Conference on Environmental Systems. San Francisco, CA: SAE International, pp. 1–12.

Iden, S., 2012. Integrated Vehicle Energy Technology (INVENT) Overview Changing the Culture through Model Based Engineering, Cincinnati, Ohio. Available at: http://ieeeusa.org/calendar/conferences/annualmeeting/2012/program/files/Friday/Track3/INVENT-Overview-Iden.pdf [Accessed January 11, 2016].

Jaworski, M., 2012. Thermal performance of heat spreader for electronics cooling with incorporated phase change material. Applied Thermal Engineering, 35, pp.212–219. Available at: http://www.sciencedirect.com/science/article/pii/S1359431111005746 [Accessed November 6, 2015].

Jones, A.B. *et al*., 2016. Thermal Sensitivity Analysis of Avionic and Environmental Control Subsystems to Variations in Flight Condition. In San Diego, CA: American Institute of Aeronautics and Astronautics, pp. 1–15.

Maxwell, D. *et al*., 2010. Thermal Survey of the EFA FCC, BAE Systems Working Paper 560/MECH/TN/2216, Rochester, UK.

Mudawar, I., 2001. Assessment of high-heat-flux thermal management schemes. IEEE Transactions on Components and Packaging Technologies, 24(2), pp.122–141. Available at: http:// ieeexplore.ieee.org/ lpdocs/ epic03/ wrapper.htm?arnumber=926375 [Accessed November 5, 2015].

Naphon, P. & Wiriyasart, S., 2012. Study on the vapor chamber with refrigerant R-141b as working fluid for HDD cooling. International Communications in Heat and Mass Transfer, 39(9), pp.1449–1452. Available at: http://www.sciencedirect.com/science/article/pii/S0735193312002096 [Accessed November 6, 2015].

Pearson, J. & McCoy, S., 2011. Thermal Management SEIC Report, BAE Systems Working Paper SEIC-RP-0981,Loughborough, UK.

Reyes, M. *et al*., 2012. Experimental and theoretical study of a vapour chamber based heat spreader for avionics applications. Applied Thermal Engineering, 37, pp.51–59. Available at: http://www.sciencedirect.com/science/article/pii/S1359431111007472 [Accessed November 6, 2015].

Söderholm, P., 2007. A system view of the No Fault Found (NFF) phenomenon. Reliability Engineering & System Safety, 92(1), pp.1–14. Available at: http://www.sciencedirect.com/science/article/pii/S0951832005002139 [Accessed November 5, 2015].

Steadman, B. *et al*., 2002. Reducing No Fault Found using statistical processing and an expert system. In IEEE AUTOTESTCON. IEEE, pp. 872–878. Available at: http://ieeexplore.ieee.org/lpdocs/epic03/wrapper.htm?arnumber=1047966 [Accessed November 5, 2015].

Strattan, L.A., 1983. Capabilities and Limitations of Air Cooled Avionic Packages. In 13th Intersociety Conference on Environmental Systems. San Francisco, CA: SAE International, pp. 1–12. Available at: http://dx.doi.org/10.4271/831105.

Teertstra, P., Culham, J.R. & Yovanovich, M.M., 1997. Calculating Interface Resistance. Electronics Cooling Magazine, pp.1–9. Available at: http:// www.mhtlab.uwaterloo.ca/ pdf_papers /mhtl97-4.pdf.

Tsai, M.C., Kang, S.W. & Vieira De Paiva, K., 2013. Experimental studies of thermal resistance in a vapor chamber heat spreader. Applied Thermal Engineering, 56(1-2), pp.38–44. Available at: http://dx.doi.org/10.1016/j.applthermaleng.2013.02.034.

Del valle, P. & Blazquez Munoz, P., 2014. Advantages of the Dynamic Simulation for the Thermal Management Systems Design. In SAE Technical Paper. SAE Technical Paper 2014-01-2152, pp. 1–8. Available at: http:// papers.sae.org/2014-01-2152/ [Accessed January 14, 2016].

Walters, E. *et al*., 2010. INVENT Modeling, Simulation, Analysis and Optimization. In 48th AIAA Aerospace Sciences Meeting Including the New Horizons Forum and Aerospace Exposition. Aerospace Sciences Meetings. American Institute of Aeronautics and Astronautics. Available at: http://dx.doi.org/10.2514/6.2010-287.

Williams, R. *et al*., 1998. An investigation of cannot duplicate failures. Quality and Reliability Engineering International, 14(5), pp.331–337. Available at: http:// dx.doi.org/ 10.1002/(SICI)1099-1638 (199809/10)14:5<331::AID-QRE183>3.0.CO.

R.G.Warsinsk, (1975) Ford develops CE cooling curve